Respiratory Physiology & Neurobiology 266 (2019) 103–114

Contents lists available at ScienceDirect

Respiratory Physiology & Neurobiology

journal homepage: www.elsevier.com/locate/resphysiol

Studying airflow structures in periodic cylindrical hills of human tracheal cartilaginous rings

Ghassem Heidarinejad[a,*], Mohammad Hossein Roozbahani[a], Mohammad Heidarinejad[b]

[a] Department of Mechanical Engineering, Tarbiat Modares University, Tehran, Iran
[b] Department of Civil, Architectural, and Environmental Engineering, Illinois Institute of Technology, Chicago, IL, USA

ARTICLE INFO

Keywords:
Human airways
Large Eddy Simulation
Kelvin-Helmholtz instability
Tracheobronchial flow
Vortical flow structur

ABSTRACT

The objective of this study is to assess tracheobronchial flow features with the cartilaginous rings during a light exercising. Tracheobronchial is part of human's body airway system that carries oxygen-rich air to human's lungs as well as takes carbon dioxide out of the human's lungs. Consequently, evaluation of the flow structures in tracheobronchial is important to support diagnosis of tracheal disorders. Computational Fluid Dynamics (CFD) allows evaluating effectiveness of tracheal cartilage rings in human body under different configurations. This study utilizes Large Eddy Simulation (LES) to model an anatomically-based human large conducting airway model with and without cartilaginous rings at the breathing conditions at Reynolds number of 5,176 in trachea region. It is observed that small recirculating areas shaped between rings cavities. While these recirculating areas are decaying, similar to periodic 2D-hills, the cartilaginous rings contribute to the construction of a vortical flow structure in the main flow. The separated vortically-shaped zone creates a wake in the flow and passes inside of the next ring cavity and disturb its boundary layer. At last, the small recirculation flow impinges onto tracheal wall. The outcome of this impinge flow is a latitudinal rotating flow perpendicular to the main flow in a cavity between the two cartilaginous rings crest which appear and disappear within a hundredth of a second. Kelvin-Helmholtz instability is observed in trachea caused by shear flow created behind of interaction between these flow structures near to tracheal wavy wall and main flow. A comparison of the results between a smooth wall model named simplified model and a rough wall model named modified model shows that these structures do not exist in simplified model, which is common in modeling tracheobronchial flow. This study proposes to consider macro surface roughness to account for the separating and rotating instantaneous flow structures. Finally, solving trachea airflow with its cartilages can become one of major issues in measuring the validity and capability of solving flow in developing types of sub-grid scale models as a turbulence studies benchmark.

1. Introduction

The fluid flow in large conducting airways has a complex nature. Except quiet breathing condition, the upper and central airways flow is turbulent or the flow is in transition from laminar to turbulent flow regimes as flow rate increases (Strohl et al., 2012). While the flow is mostly laminar at the inlet, as the flow passes downstream it becomes turbulent after the laryngeal jet, where both the local velocity and the local Reynolds number (Re) increase significantly (Kenjeres and Tjin, 2017). Solving for a laminar flow reduces the complexity of simulations (Yang et al., 2006). Because the airway sections are relatively short compared to their diameters, the airflow in the respiratory airways is not generally fully developed. This further complicates mathematical analysis and modeling of human airways (Hogberg et al., 2010). The current state-of-the-art studies have investigated the rest and sedentary conditions. Modeling under these conditions lead to the assumption that the airflow is steady in the central airways and a laminar formulation solution or only modeling the flow fluctuations by a time averaged method are sufficient (Elcner et al., 2016; Qi et al., 2014; Sul et al., 2014, Kim et al., 2017, Zheng et al., 2017). This paper plans to demonstrate the impacts of considering instantaneous turbulent flow structures that are typically represented with laminar or time averaged turbulence models and do not survive long for the light to moderate level of activity exercises. Consequently, the aim of this paper is to modify an anatomical model to provide conditions close to a more realistic condition.

In case of airflow study in the human lung, geometry and nature of the flow render the analysis complicated (Mead-Hunter et al., 2014;

* Corresponding author at: P.O.B. 14115-143, Tehran, Iran.
E-mail address: gheidari@modares.ac.ir (G. Heidarinejad).

https://doi.org/10.1016/j.resp.2019.04.012
Received 31 December 2018; Received in revised form 31 March 2019; Accepted 22 April 2019
Available online 24 April 2019

Guha et al., 2016). Current studies rarely considered these computational challenges (Guha et al., 2016). A laminar or steady state flow assumption does not account for the inherent flow complexities in upper and conducting airways. Consideration of these conditions is suitable only to model lower airways and gas interchanging bubbles alveolus flow analysis. Also, part of the complexities is due to the geometrical deformation, which is almost ignored. That is happened when the lung wall is smoothed in CAD modeling stages and the airway surface is assumed to be smooth (Xi et al., 2013). The most critical step to simulate a realistic lung model is to account for the wall macro scale natural deformation. The complexities associated with the geometry are among the significant reasons for the flow instabilities. These complexities become more complicated when the local Reynolds number of the flow approaches its critical state, which means the laminar flow is in transition to a turbulent state.

Hills shaped surfaces are one class of curved-surface configurations that has received considerable attention previously in Computational Fluid Dynamics (CFD). Streamwise periodic hills configuration involves wake flows separation. This kind of flow establishes a small recirculation area behind of the hills and converts into a 3D vertical wake of high level of unsteadiness (Castagna and Yao, 2012). Thus, this study gradually takes into account the deformations with adding the cartilages including cylindrical tandem hills.

The 2D hill configuration is specifically studied as a benchmark case (The Test Case 9.2 of the ERCOFTAC SIG 15 (Kornhaas et al., 2008) and ERCOFTAC Test Case 81 (Schroder et al., 2015; Kahler et al., 2016) for computing separated flows and developing subgrid scale models in the Large Eddy Simulation (LES). (Coelho and Pereira, 1992) represented the performance of the κ–ε eddy viscosity model by computing 2D and 3D flow over a hill. They assessed the model drawbacks in predicting turbulent flows over surface-mounted hills. Breuer et al. numerically and experimentally studied the turbulent statistics of an array of 10 hills in streamwise direction and a large spanwise extent of the channel for a Reynolds number between 700–10,595 (Breuer, 2009) They illustrated that the development of the shear layer past the hill crest is delayed; thus, a shifted downstream at Reynolds number of 700 compared to 10,595. In their study, it is revealed that a phenomenon similar to splatting phenomena occurs and the large-scale eddies generated in the shear layer of the boundary layer with the main flow, become convected in main flow.

There is an important difference between flow solving on a series of 2D and 3D tandem hills and cartilage-ring tracheal stenosis. In the investigation of tandem hills, it is necessary to utilize fine grids close to the hills especially when the hills are located just on the floor of channel. However, the grid size increases when the tracheobronchial flow is under simulation. This causes the flow to be completely surrounded by periodic cylindrical hills. This fine grid next to the wall increases accuracy of solving the tracheobronchial flow in the boundary layer zone, especially when a Lagrangian particle tracking method is applied to track the particle dispersion or deposition. However, this simulation method increases the computational costs drastically and necessitates time step size bellow 10^{-4}s. A tradeoff is to benefit from Wall modeled-LES methods. Also, the study of turbulent flow over the wavy-wall in open and closed channels or turbulent flows over rough surfaces is similar to the reviewed studies. Most of studies in these cases considered the instantaneous structure and separated flow within one wavy side of a channel, or just on a wavy plate. Vortical structures have been reported in these studies, leading to a complex flow (Zenklusen and Kuhn, 2012). As an example, Yang and Shen captured and studied this coherent vortical structures in a turbulent Couette flow over the surface wave (Yang and Shen, 2009)

Beyond the nature of air flow, the lung airways branching structure also adds further physical complexity to the analysis. This complexity shows up in different flow rates in the left and right bronchi and ultimately the smaller branching airways. It sometimes seems to be accurate just to model from CT scan images, but this approach has inherent limitations, such as requiring smoothing the walls from natural deformations and cartilages. Hence, this is followed by assessing the geometric complexities influence in the solving process. Pervious analysis proved that the flow field of the inhaled aerosols as well as the deposition patterns and the related biological effects strongly depend on the geometry of airways (Farkas, 2002).

Even though there are few studies that have investigated the effects of these geometrical complexities in airways, these studies are more focused on inhaled particle deposition rate (Akerstedt et al., 2010; Zhang and Finlay, 2005; Li et al., 2007; Wang et al., 2017). (Akerstedt et al., 2010) studied the deposition of nanoparticles in a pipe of a cartilaginous ring structure and assumed a laminar flow which is in general turbulent.

To the authors' knowledge, Evans and Castillo are among the few researchers that experimentally considered flow structure study with the consideration of cartilages effects (Evans and Castillo, 2016) Evans and Castillo mentioned while inhaled particle deposition information is very valuable, it is necessary to understand the underlying characteristics of the flow in order to reveal the deposition mechanics. In the biofluid mechanics, (Doorly et al., 2002) assessed the vortical flow structure effect on the flow transport in arteries similar to periodic hills studies. They found that the interest in vortices are quite persistent in a moderate to large Reynolds numbers (Re) in larger arteries. The presence of vortices in a flow may strongly influence its flow behavior although tracking vortices may be difficult as they can evolve in a rapid manner. The effect of vortices or vortical structures are evident when both flow stability and the processes of mixing and transport by the flow are involved.

Few studies considered unsteady flow over a rough-wall lung model; unfortunately, previous studies did not focus on the effects of macro roughness on the flow structure along tracheobronchial flow. Most of these studies investigated the cartilage rings effects on the particle deposition experimentally and a few numerically. In the discrete phase model, track of particles depend on the flow solution accuracy. For instance, it is valuable to focus on the flow close to the wall regions in numerical simulation to capture particles trapped on the walls. The periodic 2D hills case is a valuable test case that entails the near wall flow around tandem geometrical deformations. This has similarities to the cartilaginous rings case. The present study includes extra complexities such as the shape of trachea, which is cylindrical and also asymmetric bronchial airway bifurcation. Overall, the aim of this study is to:

1 Develop a realistic geometry of a human trachea model based on anatomical models
2 Prepare an accurate approach to model aerosol deposition prediction in discreet phase within considering large eddies in flow simulation
3 Show the tracheal flow is a suitable, valuable and more complicated benchmark than the periodic 2D hills to turbulence modeling and simulation
4 Focus on the dynamics of turbulent flows to develop new measures and identify vortical structures and provide insights to enhance the future eddy-particle interaction models.

2. Geometry

2.1. Geometry models

In general, there are two approaches to model the lung: (1) realistic modeling through CT scan or MRI image and (2) human lung modeling based on anatomy. The modeling through CT scan or MRI image depends on the limitation of CT scan or MRI image resolution and modification required to present the anatomical model. The early symmetric models of Weibel (Weibel, 1963) and the asymmetric model of Horsfield (Horsfield et al., 1971) are the common research contributions

investigated on assessing the airflow patterns and particle deposition through published anatomical models of the airways.

The CFD techniques are mostly applied to simulate idealized and simplified airway models (Paz et al., 2013; Brouns et al., 2007) Xi and Longest (Xi and Longest, 2007) showed using real geometry provides accurate predictions of local particle deposition. Modelling realistic geometries is essential to provide insights on the breathing process behavior. The Weibel model is more simplified than Horsfield's model; consequently, the aim of this paper is not only on the importance of realistic model based on CT scan but also to study the flow features with the consideration of the real complexities. Therefore, the use of modified anatomical model is the best choice to account for its complexity. Another complexity in modeling the geometry from CT is associated with the deviation of transforming geometry models with various extensions. For example, a transformation of a Digital Camera Images (DCIM) or Stereo lithography (STL) geometry to Standard for the Exchange of Product model data (STEP) or Standard for the Exchange of Product model data (IGES) typically lead to variation in the geometry model. Overall, the results of this study quantifies tradeoffs of using CT scan based model with more complexity, mesh cells, and computational cost.

2.2. The selected geometry model

Cartilaginous rings have impacts on the airflow in airways and inhaled particles deposition rate. The present study emphasizes on the flow features around the periodic semi cylindrical hills in an unsteady numerical manner with the consideration of reasonable mesh size and computational cost. Consequently, this study considers the Horsfield model in comparison to the Weibel model, which is applied in an asymmetric planar model (Monjezi, 2012). Cartilaginous Rings are of the highest roughness and deformation at the pulmonary and cause instabilities in the airflow. To the best of the authors' knowledge, (Martonen et al., 2000) is one of the first studies on cartilaginous rings on tracheobronchial flow, they considered some states of the ring shapes and compared the velocity profile. These rings are added to Weibel model by (Zhang and Finlay, 2005). This modification on the Horsfield model is made by (Li et al., 2007). The configuration and number of rings from Zhang's study are inputs for the present study. The maximum length of hill crest is 0.75 mm, while the trachea diameter is equal to 16 mm. As Fig. 1 shows fourteen rings are spaced evenly along the inner wall of the trachea to create the modified model. A comparison between Fig. 1(a) and (b) indicates the tracheal wall in the simple model is smooth and the modified has the cartilages. Fig. 1(c) provides a close view of the tracheal wall with the cartilages. As this figure clearly shows there are significant differences in trachea region between the simple model and the modified model.

An experimental comparison of the flow features in an idealized smooth trachea model and a second model with a roughness simulating cartilaginous rings is made by (Evans and Castillo, 2016). They applied refractive index-matched Particle Image Velocimetry (PIV) to measure the velocity field in the large conducting airways. The results for the Reynolds number of 2,600 reveals that there are considerable differences between both cases. The most important difference is the size and magnitude of recirculation zones at the inlet of both bronchi. The smooth case displays a higher vorticity along the bottom walls of the bronchi while in the case of ringed model a higher vorticity is observed along the trachea walls. These findings indicate there is a need to model the trachea using the cartilaginous rings and not the smooth tubes since the flow conditions in the lower generations are subject to the differences revealed above. Finally, (Zhang and Finlay, 2005) used experiments to show the deposition efficiency in the trachea increases significantly in the presence of cartilaginous rings. They indicated that cartilaginous rings may constitute a critical element to be integrated into future modelling of airways for the purpose of more accurate predictions on particle deposition.

3. Boundary conditions and numerical model

3.1. Physical parameters

This study considers the Semi-Implicit Method for Pressure-linked Equation (SIMPLE) algorithm to couple the pressure field and velocity field assuming an incompressible flow solver. Table 1 provides details of the physical parameters. Flow has a Reynolds number of 5176, which is comparable to a light exercising state breathing conditions.

3.2. Inlet boundary condition

Inlet and outlet mass flow rate is used from Horsfield data. The normal mass flow rate direction towards boundary is used for obtaining the inlet pressure conditions. Then, the calculated averaged pressure magnitude located at inlet and outlets facilitate the convergence rate of the simulation at the inlet mouth and nose nasal influence the inlet boundary condition in center airways. Also, pharynx and larynx regions have significant impact on the flow intensity upon entrance to trachea, which is not normally considered in human respiratory tract modeling (Akerstedt et al., 2010).

The effect of the laryngeal jet on intratracheal particle deposition has become a major concern among some researchers (Katz et al., 1999; Lin et al., 2007; Xi et al., 2008; Comerford et al., 2013; Cui et al., 2018; Bates et al., 2017).

The findings of the reviewed studies indicated that the in vitro deposition data approach in vivo measurement result only when a larynx effect is applied. Due to the increasing cost of adding the pharynx and larynx geometry to the solution domain, this study implements this effect in the inlet turbulent intensity.

Lin et al., 2007, assessed the relative importance of the upper and intra-thoracic airways and their contribution in determining central airflow patterns with major emphasis on the importance of turbulence.

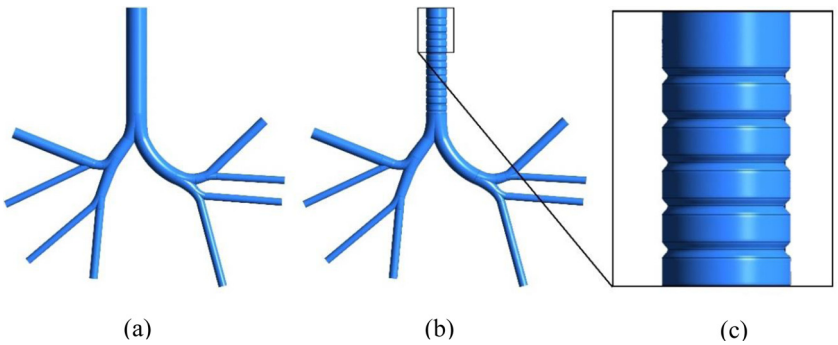

Fig. 1. Horsfield model of human lung airways: (a) simple model, (b) modified model with the fourteen rings as trachea cartilages, and (c) close view of the modified model.

Table 1
Physical parameters considered in this study.

101 kPa	Operation pressure
Physical properties	
1.2 kg/m^3	Density (ρ)
1.7 × 10^{-5} kg/ms	Viscosity (μ)
6,876,324	Number of nodes and cells
4.70 m/s	Inlet velocity
5176	Reynolds Number (Re)

Their findings indicate that turbulence induced by the laryngeal jet could significantly affect airway flow patterns and the tracheal wall shear stress. They indicate that turbulence intensity in the trachea varying from 10% to 20%. The present study created a pre-investigation model with 3 million cells and SST k-ω. This model was assessed with difference inlet turbulence intensity equal to 1, 3, 5, 7, 10 up to 20 which indicated that magnitude between 3–7% yield to 10%–20% turbulence intensity in tracheal flow. This is similar to (Lin et al., 2007) study that assumed 7% turbulent intensity located at the inlet.

3.3. Outlets condition

Even though (Choi et al., 2009) and other researchers (Katz et al., 1999; Lin et al., 2007; Xi et al., 2008; Comerford et al., 2013; Cui et al., 2018; Bates et al., 2017) examined the effects of upper airway truncation on downstream airflow, it is not well-established how modeling a reduced number of outlet branches affects the downstream airflows. (Sul et al., 2014) simulated airflows using the bronchi, central, and central–peripheral airway models and compared their flow patterns. Their results show that reduced branch geometries with appropriate boundary conditions are acceptable in modeling lung airways if the region of interest is not at the outlet branches. Since the current study's focus is on the trachea, except one boundary condition, weighted average mass flow rate is provided for all outlets as a target. The exception is for the zero average static pressure to avoid redundancy in boundary condition. Outlet mass flow rates are based on data obtained from (Horsfield et al., 1971). Another candidate was outflow in outlet boundary condition but resulted in unrealistic pressure drops (Yang et al., 2006; Sul et al., 2014) which is tested and understood in this study.

3.4. Wall boundary condition

No-slip boundary conditions are set for velocity at solid boundaries of the computational domain. This is a reasonable assumption due to the existence of mucus on the airway walls. Koombua and Pidaparti (Koombua et al., 2008) found that tissue flexibility only affects the maximum airflow velocity, airway pressure, and wall shear stress by 2%, 7%, and 6%, respectively. Thus, the assumption of wall as a rigid surface is a reasonable approximation. Fig. 2 shows the mass flow inlet and 8 mass flow outlet boundary conditions with the CFD mesh details.

3.5. Description of mesh parameters

In LES, the separation of large and small-scale turbulent fluid motions is made by applying a low-pass filter to the Navier-Stokes equations. In conventional LES, the filtering operation is applied to the Navier-Stokes equations in an "Implicit" manner. One of the outstanding drawbacks in the conventional "implicit-filter" LES is the fact that the simulation result highly depends on the applied numerical grid, due to the inherent dependency of the filtering operation on the numerical discretization. This fact indicates that this 'grid dependency' in implicit-filter LES is sensitive to the numerical errors (Tian and Ahmadi, 2012). By adopting the implicit methods in LES filter, a mesh independency could not be studied and more finer cells solved more eddies. This is due to the dependence of the filter on the grid sizes: Δx, Δy, and Δz. The benefit of this approach is with the decrease of the grid size, the filter size also becomes smaller. Thus, with a smaller filter size additional eddies are solved. Therefore, the accuracy of the simulation increases.

The fineness of mesh applied close to the walls in this study is an essential factor. The presence of recirculating bubble behind the cartilaginous rings made the flow very sensitive to the grid resolution. The flow through the Horsfield model of 3 generations by RANS is mesh independent with 1.2 million cells, but when the Horsfield model is upgraded by Periodic Cartilaginous Rings (PCRs) the count of the cells can reach to 2 million.

Calmet et al. employed 44 and 350 million cells grid within a model including the nasal cavity, oral cavity, pharynx, larynx, trachea, and partial bronchi (Calmet et al., 2016). Their results indicated that both mesh resolutions provided similar results in the inertial sub-range; however, finer mesh resolution is more useful in spectrum of flow fluctuations study than the coarse mesh. Therefore, for trachea and the next three generations, this study uses a hybrid grid with a total of 6,876,324 elements focused on the trachea. Fig. 2(b) and (c) shows the grid in the cross-section of trachea.

3.6. Solution method

According to (Li et al., 2007) transition to turbulence mode may occur at a Re = 2000 for steady flow in a straight tube. (Kleinstreuer and Zhang, 2003) and (Zhang and Finlay, 2005) reported that the flow in the human upper airways, including G0–G3, may change from laminar to turbulent flow under normal and elevated breathing conditions. Thus, there is a need to develop a numerical model that can predict low Re number laminar–transitional–turbulent flow. RANS is widely used in many studies to simulate airway turbulence. RANS models solve only the mean velocity field while the unsteadiness is averaged out. This indicates that turbulent structures are completely absent, and they are simply represented by the Reynolds stress tensor.

It is shown that the current LES model is capable of high accuracy close to Direct Numerical Simulation (DNS), which is not obtained by RANS, for the large airways airflow under normal breathing conditions (Lin et al., 2007) Also, Luo et al. reveal that particle deposition is affected mainly by large eddies, and it is reasonable to assume that LES is able to provide sufficient information for calculating particle trajectories (Luo and Liu, 2008). The Navier-Stokes equations with an added turbulent/SGS viscosity formulation is used here which are written as bellow:

$$\frac{\partial \bar{u}_i}{\partial x_i} = 0 \tag{1}$$

$$\frac{\partial \bar{u}_i}{\partial t} + \bar{u}_j \frac{\partial \bar{u}_i}{\partial x_j} = -\frac{1}{\rho}\frac{\partial \bar{p}}{\partial x_i} + \frac{\partial}{\partial x_j}\left[(\nu + \nu_T)\left(\frac{\partial \bar{u}_i}{\partial x_j} + \frac{\partial \bar{u}_j}{\partial x_i}\right)\right] \tag{2}$$

Where $\nu = 1.7 \times 10^{-5}\frac{m^2}{s}$, $\rho = 1.2\frac{kg}{m^3}$ and ν_T is equal to turbulent RANS viscosity ($\nu_T = \nu_t$) close to the wall most of time in the inner region, otherwise $\nu_T = \nu_{SGS}$.

This study uses the algebraic Wall Modeled large eddy simulation (WMLES) model. Turbulent flow entails eddies with a wide range of length and time scales. The largest eddies are typically comparable in size to the mean flow and characteristic length. The smallest scales are responsible for the dissipation of turbulence kinetic energy. In LES, large eddies are resolved in a direct manner, while small eddies are modeled. The LES, in terms of the fraction of the resolved scales, falls between DNS and RANS. Therefore, LES is more economical and efficient than DNS due to lower required computational time and resources (Cui et al., 2018). The number of grid points used in the WMLES was several hundred times lower than that of direct simulations. WMLES is proposed by (Shur et al., 2008) In the WMLES model, the eddy viscosity

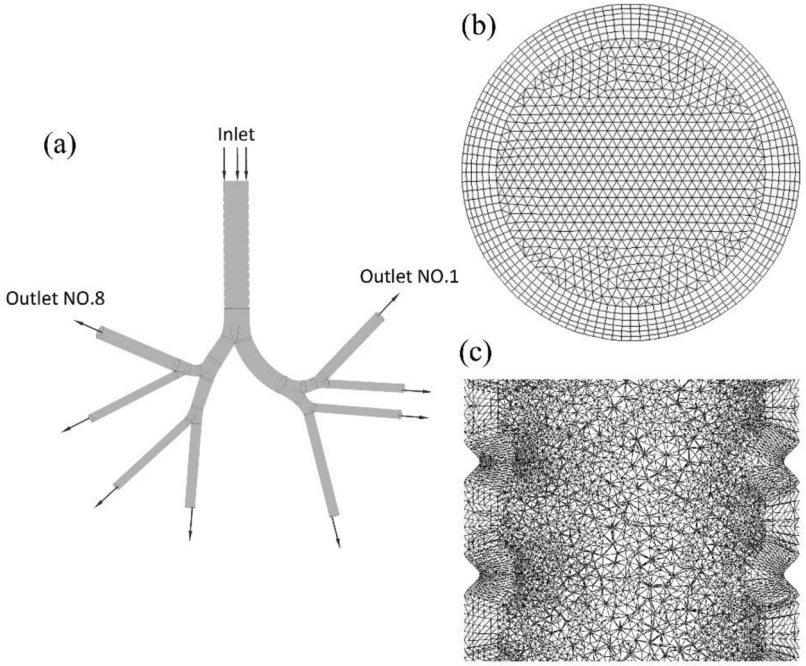

Fig. 2. Computational domain: (a) A view of the geometry of models with inlet and 8 outlets, (b) Hybrid mesh at the inlet of trachea, and (c) a close up on the cartilages curve.

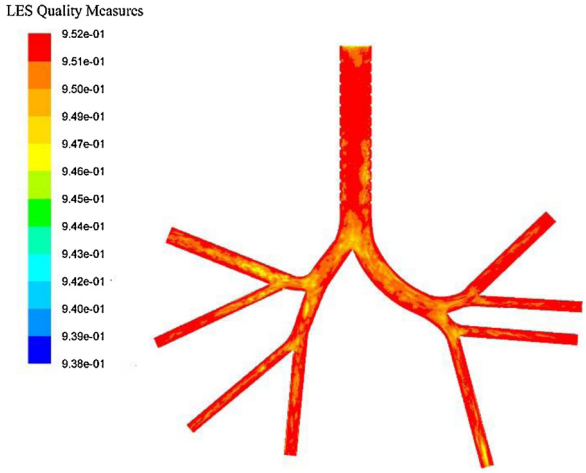

Fig. 3. The contour plot of the LES quality index.

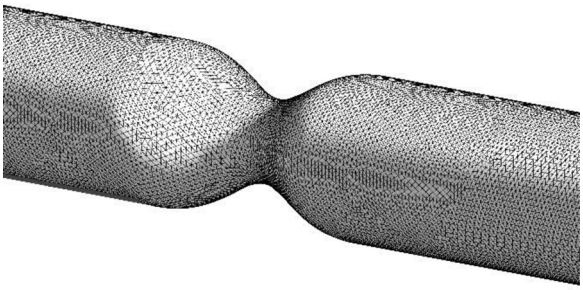

Fig. 4. The stenosis tube test-case considered for validation measured by Ahmed and Giddens (1983).

is calculated with the use of a hybrid length scale:

$$\vartheta_{SGS} = \min[(\kappa d_w)^2,\ (C_{SMAG}\Delta)^2]. \left\{1 - exp\left[-\left(\frac{y^+}{25}\right)^3\right]\right\}. |s-\Omega| \quad (3)$$

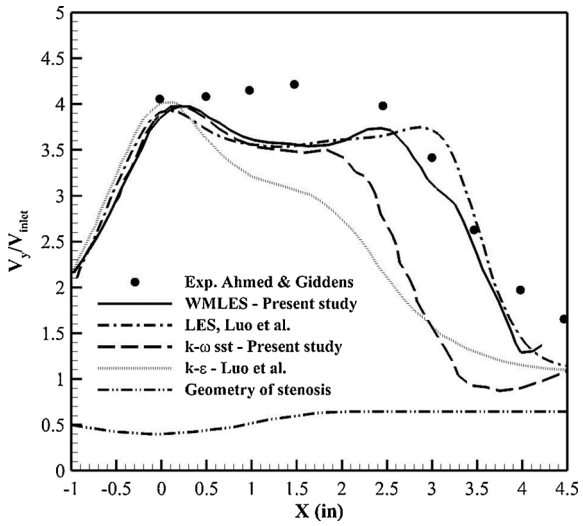

Fig. 5. Comparison of the normal centerline velocity distribution obtained using SST k–ω, and WMLES models with the experimental data by Ahmed and Giddens (1983) and Smagorinsky LES and k–e numerical result by (Luo et al., 2004).

$$\Delta = \min\{\max[C_W d_W,\ C_W h_{\max},\ h_{Wn}],\ h_{\max}\}\ C_W \approx 0.15 \quad (4)$$

Where d_w is the wall distance, κ is the von Karman constant and is equal to 0.41, y^+ is the normal to the wall inner scaling, s is the strain rate and is the magnitude of the strain tensor, Δ is the subgrid length-scale defined. C_{SMAG} is equal to 0.2, h_{max} is the maximum edge length of the cell; h_{Wn} is the wall normal grid spacing. A more detailed discussion can be found in the works by (Shur et al., 2008).

Spectral synthesizer based on Random Flow Generation method (RFG) modified by (Smirnov et al., 2001) is applied for the inflow turbulence generation method.

3.7. LES quality measures

While implicit filtering is applied, a grid-independent solution

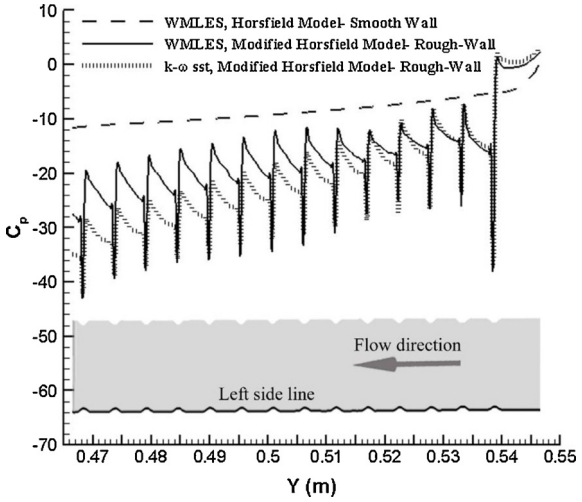

Fig. 6. Pressure coefficient along the tracheal cartilages surface at the center–plane z = 0 for all 3 test cases.

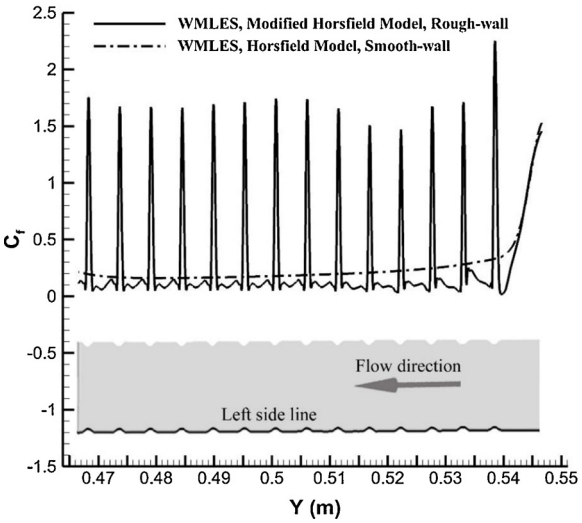

Fig. 7. Skin–friction coefficients along the tracheal cartilages surface at center–plane z = 0 in Horsfield and modified geometry models within WMLES.

cannot be achieved. To find the grid is suitable to LES or not, it is necessary to evaluate the amount of turbulent kinetic energy (Gousseau et al., 2013). The LESIQν relates the turbulent viscosity to the laminar viscosity through the following equation:

$$LESIQ_{\vartheta} = \frac{1}{1 + 0.05(\frac{(\vartheta + \vartheta_t)^{0.53}}{\vartheta}} \quad (5)$$

The $LESIQ_{\vartheta}$ is a non-dimensional number between zero and one. The constants are calibrated in a manner that the index behaves similar to the ratio of resolved to total turbulent kinetic energy, i.e. (E_{LES}/E_{DNS}). An index of quality greater than 0.85 is considered as an appropriate LES. According to above equation here the minimum of $LESIQ_{\vartheta}$ earned 0.93. A contour of $LESIQ_{\vartheta}$ is shown in Fig. 3. This is due to the advantages of tiny cells and the fine mesh which allows the PRISM boundary layer mesh to be close to the walls and this makes the filter length about 1.884×10^{-4}. Averaged courant number in all domains is smaller than 0.35.

4. Validation

Except few datasets about particle deposition rate, there are limited previous published experimental studies on the flow characteristics in the Horsfield model or modified model. Therefore, the velocity field in a stenosis tube measured by (Ahmed and Giddens, 1983) serves as the validation case study for the LES simulation. Luo XY., et al. (Luo et al., 2004) applied LES to solve the flow in the upper airway and validated with the Ahmed and Giddens's experimental data. The present study validates the simulation results with two different studies: (i) the case when Re = 2000 with the experimental data presented by Ahmed and Giddens (Ahmed and Giddens, 1983) and (ii) numerical results available from (Luo et al., 2004) for a model diameter of 0.0508 m in the unobstructed part. Similar to the airway simulation, both RANS and LES are applied with similar boundary conditions and methods. The value of turbulence intensity at the inlet of the pipe is 6.18% in order to represent the turbulent flow regimes similar to the experiment presented in (Ahmed and Giddens, 1983). As Fig. 4 shows the calculations use a 7,680,324 cells grid. The computational domain is extended to 10D where inlet velocity (V_{inlet}) in the boundary condition is 0.3 $\frac{m}{s}$.

Computational results are compared for the normalized velocity, V_x, to the mean time-averaged velocity ($\bar{V}$), on the mid-line in the tube stenosis. As it is shown in Fig. 5, the presented WMLES approach in this study provides results within a good agreement with the measurements (e.g. Luo et al., 2004) when a Smagorinsky subgrid scale model (SGS) for the LES has been used. The results of two other models differ most significantly from the experimental data. As Fig. 6 illustrates the RANS calculations do not have an accurate representation of the Reynolds stress tensor specifically within the separated flow over the stenosis. This yields in inaccurate results as for the SST k-ω in this study and k-ε model from (Luo et al., 2004) studies. The k-ε model has reasonable accuracy for a wide variety of flows without separation. Hence, it appears to underestimate the flow where the SST k-ω model predicted close to LES. Finally, it has been found necessary to use LES approach, considering the effect of vortical flow structure and to simulate the large-scale unsteady vortex structures.

5. Results

Fig. 6 illustrates the computed mean surface streamwise pressure

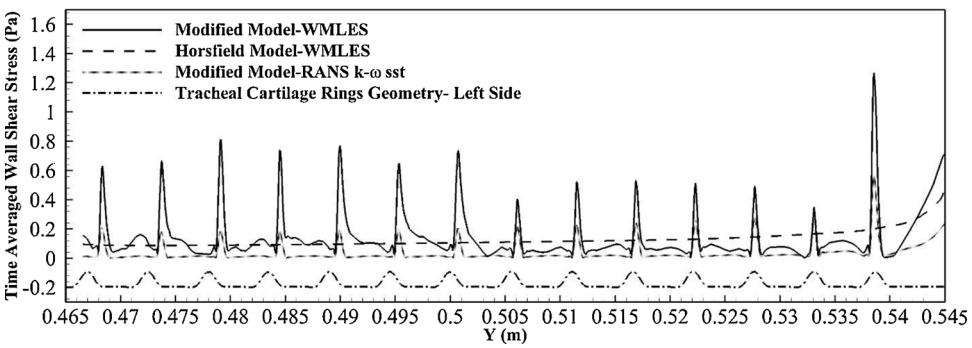

Fig. 8. The variation of wall shear stress along the tracheal cartilages surface at a line on the center–plane z = 0 in the flow direction (right to left).

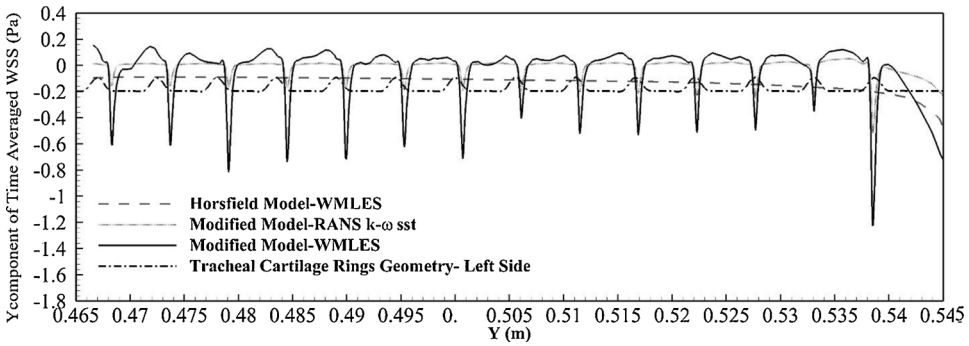

Fig. 9. The Y component of wall shear stress along the tracheal cartilages surface at a line on the center–plane z = 0 in the flow direction (right to left).

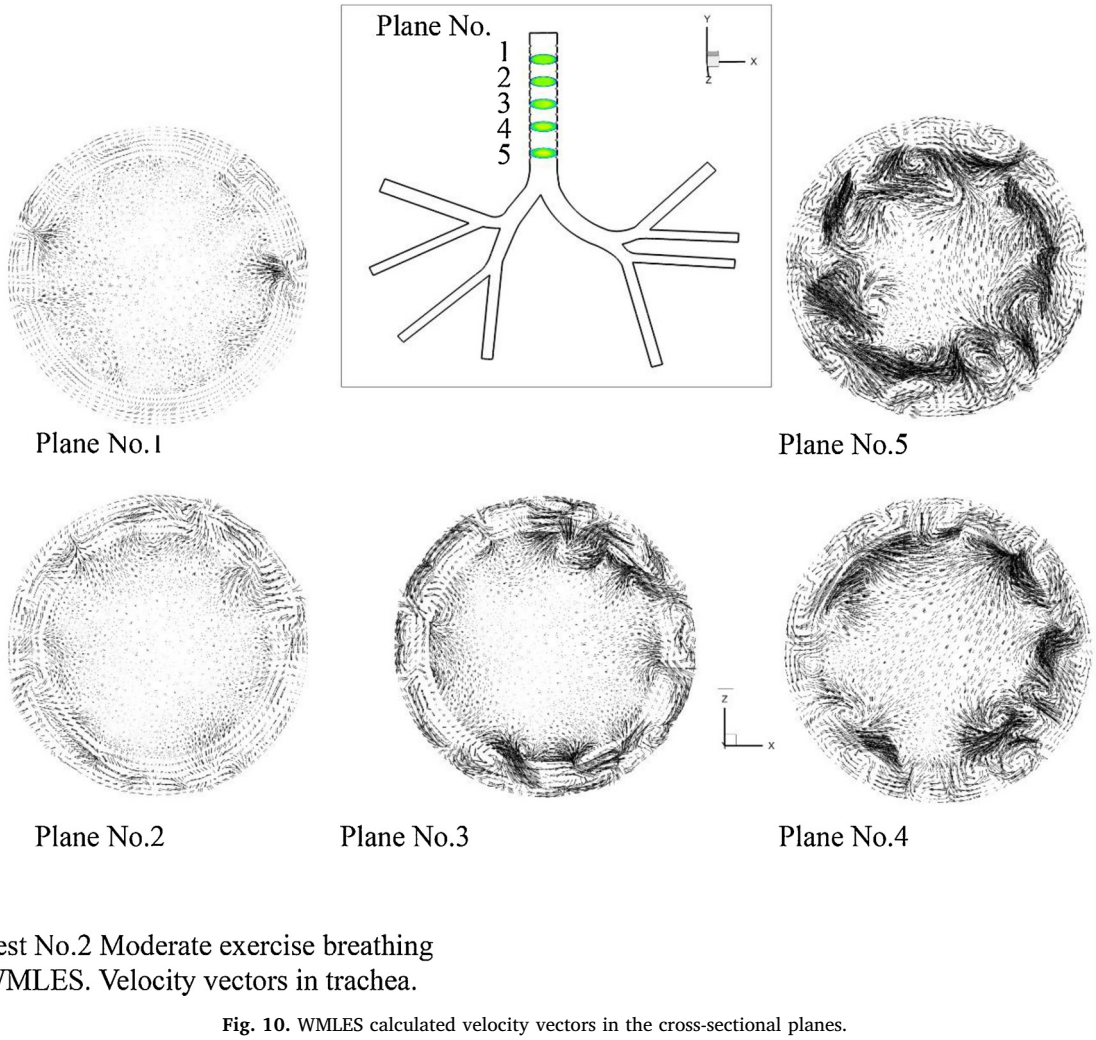

Fig. 10. WMLES calculated velocity vectors in the cross-sectional planes.

coefficient (C_p) distributions along the left side line of the tracheal wall. In the smoothed model, flow passes through without any especial feature except secondary flows; however, in the modified model, due to the existence of cartilaginous, flow is unsteady especially close to the walls and between the cartilaginous rings distance. The pressure coefficient values started from 2.47 in the inlet and decreased as flow passed down into trachea but in each interaction by the cartilages face increased. Eqs. (6) and (7) provide the pressure (C_p) and skin fraction (C_f) coefficients.

$$C_p = \frac{p - p_\infty}{\frac{1}{2}\rho u_b^2}, \tag{6}$$

$$C_f = \frac{\tau_w}{\frac{1}{2}\rho u_b^2} \tag{7}$$

Where p is the local pressure, p_∞ is atmospheric pressure, ρ is the airflow density, τ_w is wall shear force, and u_b is the local velocity.

As Fig. 6 shows for WMLES the maximum value of pressure coefficient is about 1.52 at the stagnation point which is the foot of first cartilage (Y = 0.5391). The most decrease in pressure occurs at the location of the cavity. C_p decreases from 1.52 corresponding with a pressure equals to 0.5955 Pa to C_p = -38.09 corresponding with a pressure equal to-23.63 Pa and Y = 0.5384 m. Also, as Fig. 6 illustrates the pressure coefficient suddenly return to a value about -25.16 corresponded with a pressure equal to -15.62. 1 Pa and Y = 0.5383 m.

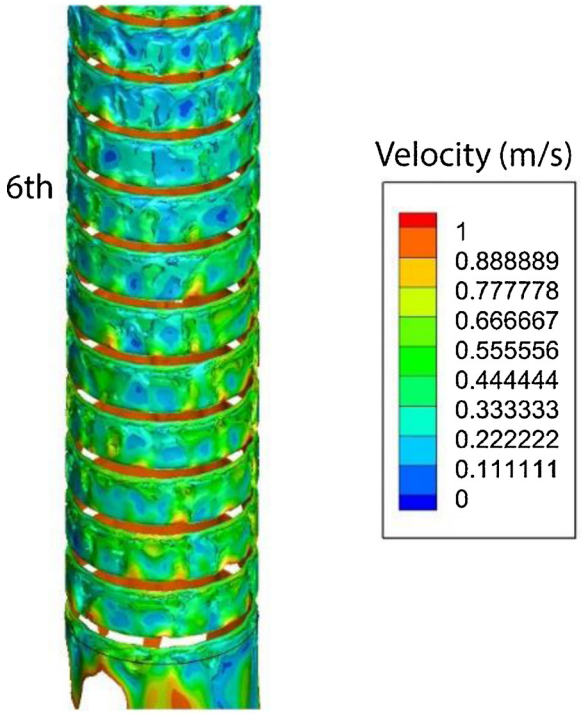

Fig. 11. Velocity contour iso-surface close to the trachea wall-between the cartilages.

Then, the C_p values increase slowly along the vortical structures wake region and recovered around the crest of the 2nd cartilage to about −9.622 (P = −10. 1 Pa & Y = 0.533 m). This oscillating pressure behavior is also repeated for subsequent cartilages.

The C_p results of the SST k-ω model follow relatively the same patterns as the WMLES results. However, the SST k-ω results have significant differences for the C_p values compared to the WMLES model. There is an increase between the region of the cartilaginous rings where the vortex structures and separated vortical flows is introduced in the flow. Fig. 6 shows that the C_p values in Horsfield model without any cartilages, and the results indicate a slow descending pattern from −0.59 to −11.6 at the end of trachea.

Similar to Fig. 6, Fig. 7 compares the skin friction distribution along a line on the left side of tracheal wall. This figure shows that adding the cartilages roughness to the trachea contributes to an increase in skin friction peaks, which is due to the additional wall shear stress values compared to the usual Horsfield model. SST k- ω model calculated lower value for the C_f peak and resulted in different flow structures from the WMLES especially in the regions between two cartilages. Overall, future studies could conduct a comprehensive study to accurately compare the simulated results with the experimental measurements using a detailed tracheal geometry.

Existence of disturbances in the flow energy leads to an increase in the magnitude of Wall Shear Stress (WSS) between the cartilaginous rings. Fig. 8 depicts this increase in the magnitude of WSS for different models. As it is illustrated in Fig. 8, even though the Horsfiled model with smooth wall is solved by WMLES approach, without the tracheal cartilages, the WSS magnitude is close to 0.1 Pa. If this test has been calculated with RANS approach, the predicted value would be significantly low as it is reported by (Zhang et al., 2016). They showed the value is about 0.0005 Pa (an order of 10-4 magnitude different) within k- ε RANS in a smooth wall. As Fig. 8 shows these very low predictions are in contrary to the maximum WSS which is equal to 1.2 Pa for the left line on the tracheal wall and 1.4 Pa for the right line when a modified geometry and WMLES are considered. (Calmet et al., 2016) also reported a WSS magnitude up to 2.5–3 Pa in the nasal cavity. They have used realistic airways geometry and LES approach.

The RANS model was unable to determine the WSS increase between the two cartilages crest in comparison with the LES results. As Fig. 8 depicts from a positive to a negative value oscillation (and conversely) of the Y component of wall shear stress, the results present the separation and reattachment points which has been shown in Fig. 9. The WMLES solution predicted 29 detached and reattached points while the RANS model predicted 27 points. Due to the unsteady nature of the flow, it is not reasonable to conduct a comparative investigation on predictions between models in the detached point and reattachment point. An accurate experimental study of flow structure in lung tracheacylindrical geometry with the cartilaginous rings is highly required to validate the actual flow patterns. According to the mentioned results, the main differences between the tips and notes mentioned in this article within modified model and the common way within existing smooth-wall airways models like Horsfield model are:

1) Additional peak values obtained for wall shear stress on the tracheal wavy wall which is critical for tracheal Epithelium cells in mechanical ventilation analyses known as artificial lung ventilation. As Fig. 8 presents the values are about 12-times higher than the WSS predicted for the Horsfield model with smooth wall.
2) A transitional flow close to the tracheal walls within the modified model, which identified a separated, detached, and reattached flow in these zones.
3) It is not enough to consider the geometrical wall deformations such as considering the tracheal cartilages but also geometrical complexities need a proper approach. For example, the modified model in RANS approach predicted a very lower value close to zero for WSS except in peak maximum which is about 0.4 Pa. This value is still significantly lower than the maximum value calculated within WMLES, which is 1.2 as Fig. 8 illustrates.

Fig. 10 shows the calculated instantaneous velocity vectors on spanwise planes in the airways obtained from LES in the presence of cartilaginous rings. From plane 1 to plane 5, as the flow passes downward along the cartilages, the spanwise velocity fluctuations are observed to be high close to the tracheal wall and as it approaches the center line, fluctuations decreased remarkably. These eddy type structures create chaotic flow behavior with high and low shear stresses even if the Re number is low in near-wall regions. Using more realistic geometry along with LES method has enabled the numerical calculations to capture impinging-type flow after some cartilages crest which have not been observed in the other numerical configurations mentioned so far. These flow structures are produced by dissipation of cavity-like flow in the recirculation zones. These structures are associated with the creation of high Turbulence Kinetic Energy (TKE) region at the mixing layer between the cavity-like flow in the recirculation zone and the free stream. These results are in qualitatively good agreement with those observed by (Koullapis et al., 2016). These planes did not have any considerable spanwise motions in common Horsfield model with smooth wall. Consideration of simplified model of airways only provides the secondary flow structures shaped after the trachea when the flow passes in curvy airways. Fig. 10 clearly shows that in an airways model more similar to realistic lung, the geometrical deformation of walls changed the flow patterns.

The magnitude of the instantaneous velocity for WMLES simulation increased up to 3 m/s between cartilages. Time averaged on the 1.4 s of these magnitude have values up to 1 m/s that is clear in the velocity counter close to the wall between tracheal cartilages in Fig. 11. LES provides a better estimation of recirculation zones caused by presence of cartilaginous rings.

Fig. 12(a) indicates that RANS predicted the size of recirculation zones as equal to cartilaginous rings distance without their associated wake separation flow. Consequently, it is not possible to investigate the reattachment locations. As these phenomena are presented in Fig. 12(b)

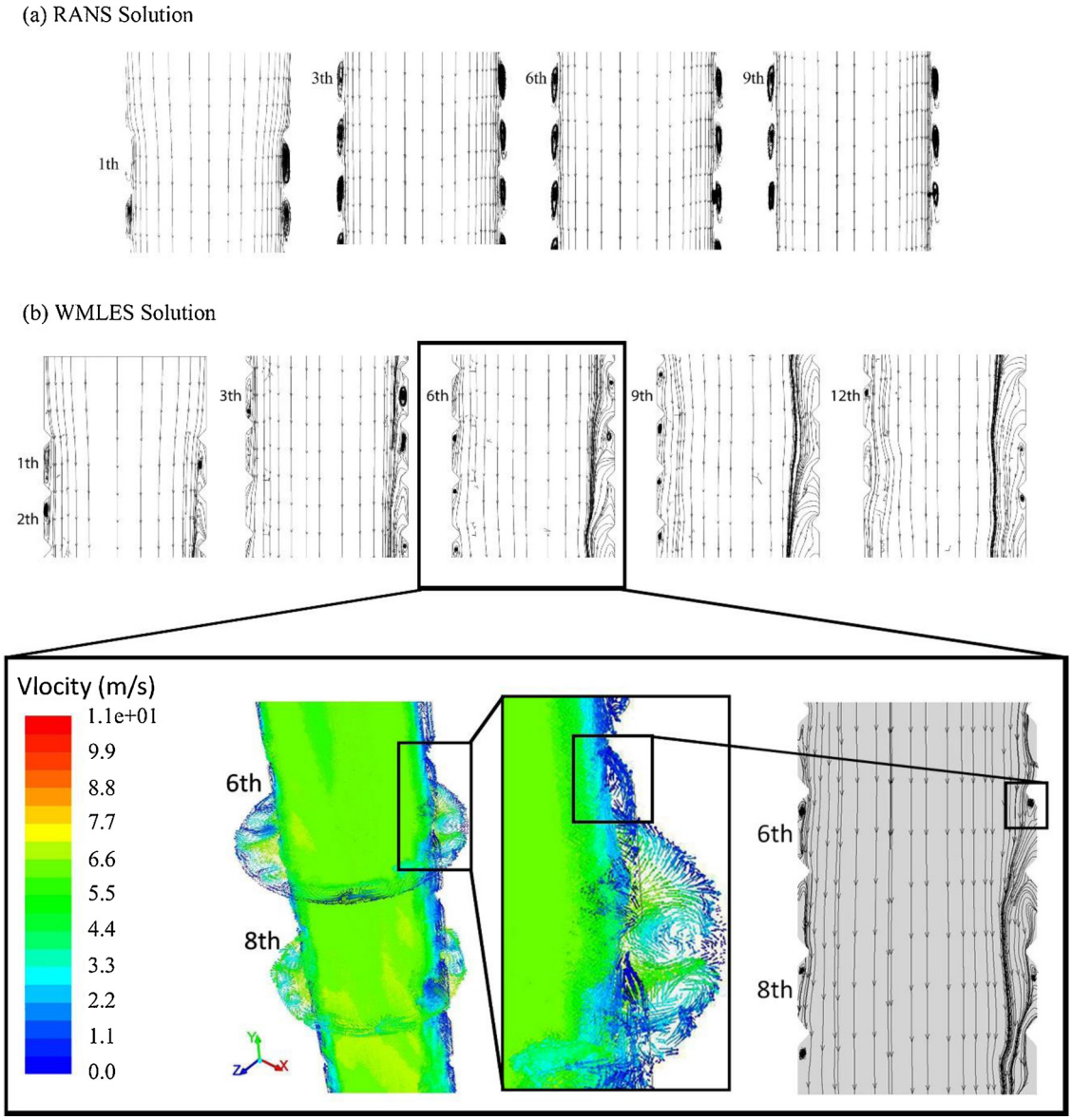

Fig. 12. Streamlines showing velocity of flow at symmetry plane (x–y) z = 0: (a) calculated by RANS, (b) calculated by WMLES, (c) calculated by WMLES with a close up view of 6th and 8th cartilages and velocity vectors showing in symmetry and cross-sectional planes correspond to each one.

and (c), the WMLES estimated flow recirculation zones smaller than cartilaginous rings distance and their size alter with time. Also, mentioned zones contributed in separating and detaching the flow. Thus, the unsteady behavior of these recirculation zones constitutes an additional difficulty in solution, which means that the steady solution of RANS is therefore ill-suited to such conditions.

6. Discussions

LES directly calculates vortex tubes greater than the mesh size and takes into account the influence of smaller vortex tubes with modeling. Previous RANS studies have mainly focused on the steady flow and ultimately the mean vortex patterns do not represent the unsteady instantaneous flow structures. Consequently, SST k-ω calculation can capture only mean vortex in each cavity between cartilages.

Recently, (Guha and Pradhan, 2017) studied six generation of a three-dimensional model of the bronchial tree network and explained the Dean vortices and anti-Dean vortices as secondary flow patterns. Their laminar flow analysis at low Reynolds number of 400 to 1000 and 1600 solved the tracheobronchial flow without any flow structures on a cross-sectional plane. The results showed that secondary velocity magnitude is small in the trachea while not acknowledging much of its complexity. Therefore, the current paper's LES simulation results using modified geometry and at a high Reynolds number of 5176 is able to capture the vortices in flow pattern on the cross-sectional planes as the inspired air traverses the trachea. Most of these vortices are formed close to the trachea wavy wall as it is shown in 5 cross-sectional planes in Fig. 10. Fig. 10 illustrates as the flow convected down over the cartilaginous rings, counter-rotating vortices are growing up where in last plane, plane 5 between 13th and 14th rings, their numbers are very large and occupy the entire area around the wall.

Fig. 12(a) shows the flow over a cartilage separated vortically from the crest as a shear layer and penetrated in the main flow with an oscillation above two next cartilaginous rings when it is solved by WMLES. This streamwise structure is not captured and stationary circulation zones are limited just to spanwise direction. If the unsteady flow was solved, this circulation zones move dynamically and disappear as passes forward between the cartilage crests. Ultimately, it causes oscillation of the very large separated wake-like flow structures up and down. Consequently, the very large scale streamwise eddies sometimes

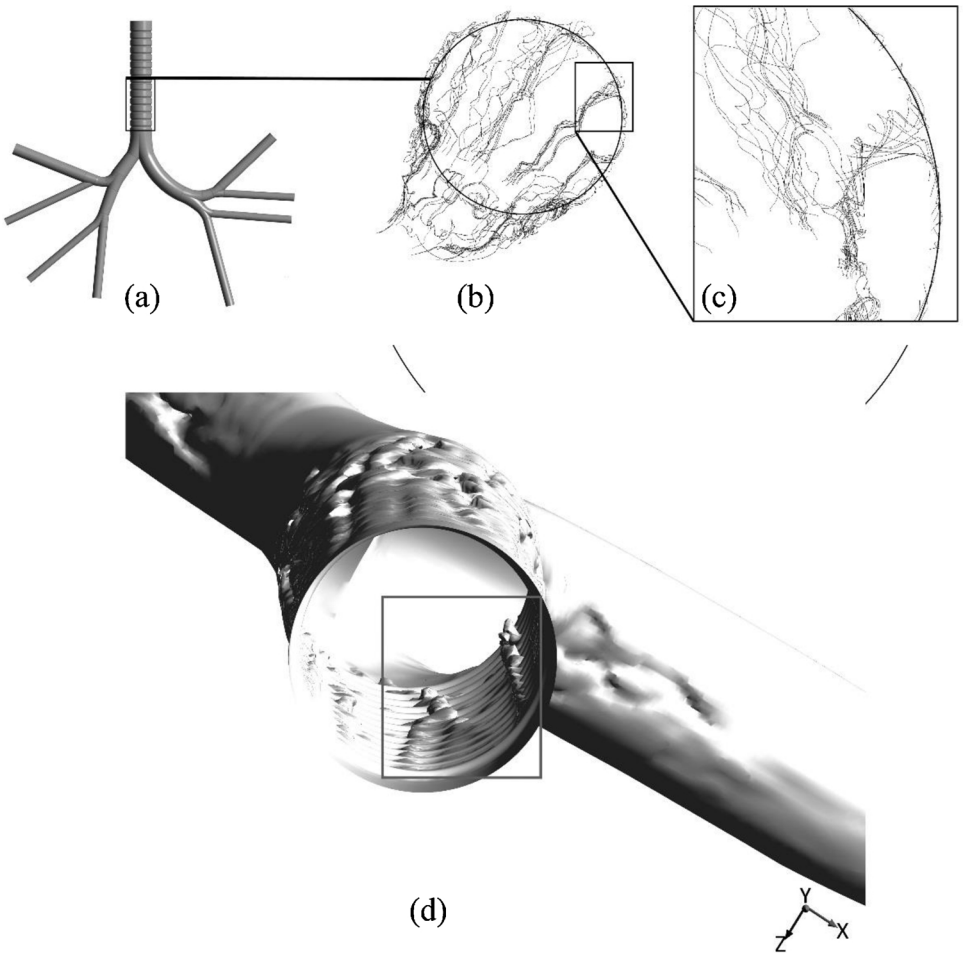

Fig. 13. (a, b) Demonstration of separated vortical wake flow by velocity streamlines over 8th cartilages and (c) focused view, and (d) an illustration of the vertical flow structures showed by 3D velocity iso-surface when V = 1.2 $\frac{m}{s}$.

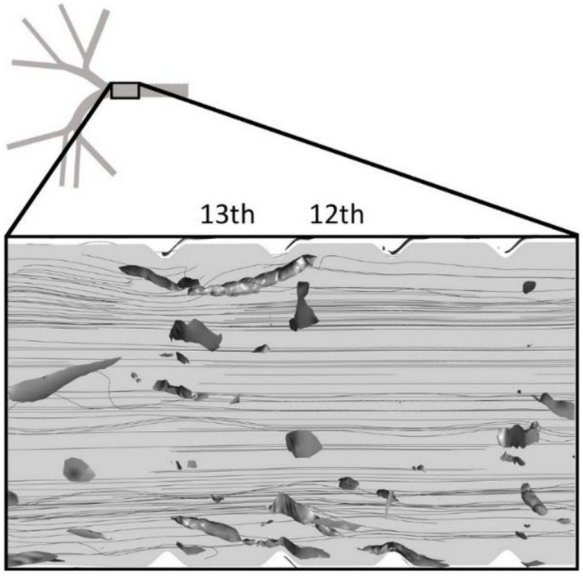

Fig. 14. An illustration of the vertical flow structures showed by 3D Y component of vorticity iso-surface at the magnitude of 5000 in a side view of the 12th and 13th cartilage with sample streamlines.

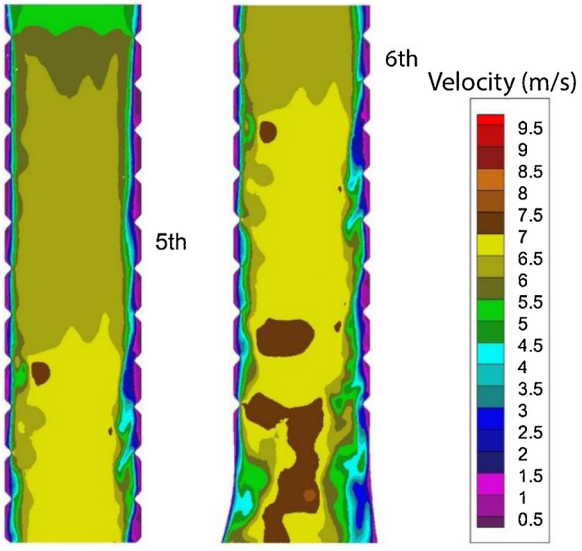

Fig. 15. Visualization of kelvin-Helmholtz phenomenon appearance in trachea by contour of velocity in two time, left hand side t = 0.17 s and right hand side t = 3.79 s.

entered in the distance of the next cartilages crests and disturbed their circulation zone and boundary layer. Fig. 12(b) depicts this instantaneous phenomenon. This pattern happens for the separated vortical flow from the 6th cavity crest oscillated above the 8th cavity which has been shown in a focused view of Fig. 12(b) along the velocity contour and velocity vectors on the spanwise planes. This focused view shows a new circulation creation in 6th cavity after that the pervious cavity (i) grew up, (ii) moved forward to the end of the cavity crest distance, and (iii) decayed while contributes to a streamwise vortical flow. Furthermore, Fig. 13 presents the long and small vortical structures. While Fig.13(a) shows the streamlines, Fig. 13(b) depicts the iso-

surface of the velocity. Flow over these cartilaginous rings obstacles experiences boundary layer separation and detached flow configuration due to very strong flow oscillations. Instantaneous 3D structures appear as thin spiral rolls along trachea walls at a relatively small and long scale.

Results showed smaller vortical structures in last cartilaginous rings than those highlighted in Fig. 13. This finding is consistent with (Calmet et al., 2016) research which noted that as the flow descends the trachea, the energy of large structures is dissipated. Therefore, as Fig. 14 shows the energy content decreases and the vortical structures are broken down into smaller ones. These small coherent vortical structures are considerably bigger than mesh cells. Thus, LES solves them especially where the flow is separated or known as low-speed very large scale motions (VLSMs). It is important to note that RANS uses wall function, so it is notable to capture these structure since these structures are inherent part of an instantaneous flow.

Instantaneous vortical structure shaped in the cartilages cavity and entered into the main flow. Because of the lower magnitude of vertical velocity, from 0.2 up to 4 m/s, compared to the main flow local velocity in trachea, 6–8 m/s, a shear flow is produced. Vortical structures and the predominant recirculation zones will affect the inhaled particle motion and subsequently their deposition pattern (Cui and Gutheil, 2018). Fig. 15 depicts this shear flow as it appears as a kelvin-Helmholtz phenomenon periodically in different times and location of the 3rd cartilaginous ring to the next rings. This is an extra phenomenon regarding airflow in upper central airways specific to the interaction between free-stream turbulence and boundary layers, which has been explained by (Hunta and Durbin, 1999). Since their studies were run on a flat plate or 2D hills, even 3D hill was located on a flat plate and was not cylindrically rounded or wall bounded as here for the lung cartilages.

7. Conclusions

This study modeled the trachea geometry using the modified Horsfield model comprised of tracheal cartilage rings in human body to account for the non-smooth airway walls. The aim of this paper was to determine the importance of natural geometric complexities and instantaneous flow structures in the airflow modeling. Therefore, this study uses Large Eddy Simulation (LES) in Computational Fluid Dynamics (CFD) to simulate the breath conditions at Reynolds number of 5176. This accurate prediction of flow solution is very important in the prediction of the pollution particles dispersion and deposition. Separated large and very large scale low-speed motions as well as secondary vortices can strongly affect the inhaled particles. The results of this study indicated that considering only a realistic geometry is not the only method to increase accuracy of the airflow perdition but also there is a need to use a suitable turbulence model. Furthermore, the results of this research are useful to the airflow-related shear stress on the epithelial cell investigation in the mechanical ventilation where the instantaneous magnitude is needed instead of a time averaged magnitude. This study showed that considering both of geometrical and numerical complexities along the trachea problem, provides significantly higher Wall Shear Stress (WSS) peak over the cartilages from 0.1 Pa in the case without geometrical complexities and 0.6 Pa while considering the geometrical complexities up to 1.2 and 1.4 Pa in the case of considering both kind of complexities.

The present study showed that the vortices formed after the cartilages leading to wake breakdown. At the same time, it is observed sometimes rapid decay of vortices accompanied to create a strong wake which affect the flow. Similarity between tracheal flow and flow over periodic hills and wavy sinusoidal wall pipe has been demonstrated by flow structure study, but there still exist some differences among them due to lung branching morphogenesis. These differences result in different flow rate between left and right lung lobes which have impacts on their flow rates. Flow enters faster in the left side of trachea so makes a little suction on right side. This is the reason why the very large scale low-speed motions as well as separation wakes are generated more in right side of trachea than those of left side.

From the results, it can be inferred that the time averaged solution such as RANS models, especially SST K-ω model, are clearly not suitable for the current case. According to the flow separation observed over all rings, wall shear stress varied from positive to negative. Then, a vortical separated flow structure as a wake from boundary layer region interacted into main flow or entered into next cavities. This large scale vortical flow has been broken down into small eddies and secondary vortices. For more investigation and ability to compare the different Smagorinsky subgrid scale models (SGSs), it is indispensable to experimentally test a cylindrical geometry with periodic hills within a branched end. This is valuable from two aspects: (i) for the breathing airflow simulation and (ii) as a benchmark more complicated than periodic 2D hills to assess the turbulence simulation and SGSs. This study recommends future studies to investigate secondary instability of boundary layer streaks known as small turbulent structures using Direct Numerical Solution (DNS) to earn a deep knowledge of tracheobronchial flow instability analysis.

References

Ahmed, S., Giddens, D.P., 1983. Velocity measurement in steady flow through axisymmetric stenoses at moderate Reynolds number. J. Biomech. 16 (7), 505–516. https://doi.org/10.1016/0021-9290(83)90065-9.

Akerstedt, H.O., Hogber, S.M., Lundstrom, T.S., Sandstrom, T., 2010. The effect of cartilaginous rings on particle deposition by convection and Brownian diffusion. Nat. Sci. (Irvine) 2 (7), 769–779. https://doi.org/10.4236/ns.2010.27097.

Bates, A.J., et al., 2017. Computational fluid dynamics benchmark dataset of airflow in tracheas. Data Brief 10, 101–107. https://doi.org/10.1016/j.dib.2016.11.091.

Breuer, M., et al., 2009. Flow over periodic hills-numerical and experimental study in a wide range of Reynolds numbers. Comput. Fluids 38 (2), 433–457. https://doi.org/10.1016/j.compfluid.2008.05.002.

Brouns, M., Verbanck, S., Lacor, C., 2007. Influence of glottic aperture on the tracheal flow. J. Biomech. 40 (1), 165–172. https://doi.org/10.1016/j.jbiomech.2005.10.033.

Calmet, H., et al., 2016. Large-scale CFD simulations of the transitional and turbulent regime for the large human airways during rapid inhalation. Comput. Biol. Med. 69, 166–180. https://doi.org/10.1016/j.compbiomed.2015.12.003.

Castagna, J., Yao, Y., 2012. Numerical simulation of a turbulent flow over an axisymmetric Hill. 50th AIAA Aerospace Sciences Meeting Including the New Horizons Forum and Aerospace Exposition Nashville.

Choi, J., et al., 2009. On intra- and intersubject variabilities of airflow in the human lungs. Phys. Fluids 21. https://doi.org/10.1063/1.3247170.

Coelho, P.J., Pereira, J.C.F., 1992. Finite volume computation of the turbulent flow over a hill employing 2D or 3D non-orthogonal collocated grid systems. Int. J. Numer. Methods Fluids 14 (4), 423–441. https://doi.org/10.1002/fld.1650140404.

Comerford, A., Gravemeier, V., Wall, W.A., 2013. An algebraic variational multiscale-multigrid method for large-eddy simulation of turbulent pulsatile flows in complex geometries with detailed insight into pulmonary airway flow. Int. J. Numer. Methods Fluids 71 (10), 1207–1225. https://doi.org/10.1002/fld.3704.

Cui, X., Gutheil, E., 2018. Large eddy simulation of the flow pattern in an idealized mouth-throat under unsteady inspiration flow conditions. Respir. Physiol. Neurobiol. https://doi.org/10.1016/j.resp.2018.03.002.

Cui, X., Wu, W., Gutheil, E., 2018. Numerical study of the airflow structures in an idealized mouth-throat under light and heavy breathing intensities using large eddy simulation. Respir. Physiol. Neurobiol. 248, 1–9. https://doi.org/10.1016/j.resp.2017.11.001.

Doorly, D.J., et al., 2002. Vortical flow structure identification and flow transport in arteries. Comput. Methods Biomech. Biomed. Eng. 5 (3), 261–275. https://doi.org/10.1080/10255840290010715.

Elcner, J., et al., 2016. Study of airflow during respiratory cycle in semi-realistic model of human tracheobronchial tree. AIP Conference Proceedings 1745. https://doi.org/10.1063/1.4953703.

Evans, H.B., Castillo, L., 2016. Index-matched measurements of the effect of cartilaginous rings on tracheobronchial flow. J. Biomech. 49 (9). https://doi.org/10.1016/j.jbiomech.2016.03.043.

Farkas, A., et al., 2002. Simulation of deposition and activity distributions of radionuclides in human airways. European IRPA Congress, Towards Harmonization of Radiation Protection in Europe.

Gousseau, P., Blocken, B., Heijst, G.V., 2013. Quality assessment of Large-Eddy Simulation of wind flow around a high-rise building: validation and solution verification. Comput. Fluids 79, 120–133. https://doi.org/10.1016/j.compfluid.2013.03.006.

Guha, A., Pradhan, K., 2017. Secondary motion in three-dimensional branching networks. Phys. Fluids 29. https://doi.org/10.1063/1.4984919.

Guha, A., Pradhan, K., Halder, P.K., 2016. Finding order in complexity: a study of the fluid dynamics in a three dimensional branching network. Phys. Fluids 28 (1994), 123602. https://doi.org/10.1063/1.4971315.

Hogberg, S.M., et al., 2010. Respiratory deposition of fibers in the non-inertial regime–development and application of a semi-analytical model. Aerosol Sci. Technol. 44 (10), 847–860. https://doi.org/10.1080/02786826.2010.498455.
Horsfield, K., et al., 1971. Models of the human bronchial tree. J. Appl. Physiol. 31 (2), 207–217. https://doi.org/10.1152/jappl.1971.31.2.207.
Hunta, J.C.R., Durbin, P.A., 1999. Perturbed vortical layers and shear sheltering. Fluid Dyn. Res. 24 (6), 375–404. https://doi.org/10.1016/S0169-5983(99)00009-X.
Kahler, C.J., Scharnowski, S., Cierpka, C., 2016. Highly resolved experimental results of the separated flow in a channel wit streamwise periodic constrictions. J. Fluid Mech. 796, 257–284. https://doi.org/10.1017/jfm.2016.250.
Katz, I.M., Davis, B.M., Martonen, T.B., 1999. A numerical study of particle motion within the human larynx and Trachea. J. Aerosol Sci. 30 (2), 173–183. https://doi.org/10.1016/S0021-8502(98)00043-3.
Kenjeres, S., Tjin, J.L., 2017. Numerical simulations of targeted delivery of magnetic drug aerosols in the human upper and central respiratory system: a validation study. R. Soc. Open Sci. 4 (12). https://doi.org/10.1098/rsos.170873.
Kim, J., et al., 2017. Aging effects on airflow dynamics and lung function in human bronchioles. PLoS One 12 (8), e0183654. https://doi.org/10.1371/journal.
Kleinstreuer, C., Zhang, Z., 2003. Laminar-to-turbulent fluid-particle flows in a human airway model. Int. J. Multiph. Flow 29 (2), 271–289. https://doi.org/10.1016/S0301-9322(02)00131-3.
Koombua, K., et al., 2008. Computational analysis of fluid characteristics in rigid and flexible human respiratory airway models. Eng. Appl. Comput. Fluid Mech. 2 (2), 185–194. https://doi.org/10.1080/19942060.2008.11015220.
Kornhaas, M., et al., 2008. Influence of time step size and convergence criteria on large eddy simulations with implicit time discretization. Qual. Reliab. Large-Eddy Simulations 12, 119–130. https://doi.org/10.1007/978-1-4020-8578-9_10.
Koullapis, P.G., et al., 2016. Particle deposition in a realistic geometry of the human conducting airways: effects of inlet velocity profile, inhalation flowrate and electrostatic charge. J. Biomech. 49 (11), 2201–2212. https://doi.org/10.1016/j.jbiomech.2015.11.029.
Li, Z., Kleinstreuer, C., Zhang, Z., 2007. Particle deposition in the human tracheobronchial airways due to transient inspiratory flow patterns. Aerosol Sci. Technol. 38 (6), 625–644. https://doi.org/10.1016/j.jaerosci.2007.03.010.
Lin, C.L., et al., 2007. Characteristics of the turbulent laryngeal jet and its effect on airflow in the human intra-thoracic airways. Respir. Physiol. Neurobiol. 157 (2-3), 295–309. https://doi.org/10.1016/j.resp.2007.02.006.
Luo, H.Y., Liu, Y., 2008. Modeling the bifurcating flow in a CT-scanned human lung airway. J. Biomech. 41 (12), 2681–2688. https://doi.org/10.1016/j.jbiomech.2008.06.018.
Luo, X.Y., Hinton, J.S., Liew, T.T., Tan, K.K., 2004. LES modelling of flow in a simple airway model. Med. Eng. Phys. 26 (5), 403–413. https://doi.org/10.1016/j.medengphy.2004.02.008. 2004.
Martonen, T.B., et al., 2000. Lung models: strengths and limitations. Respir. Care 45 (6), 712–736.
Mead-Hunter, R., et al., 2014. Simulation of respiratory flows. 19th Australasian Fluid Mechanics Conference.
Monjezi, M., et al., 2012. Prediction of particle deposition in the respiratory track using 3D–1D modeling. Sci. Iran. 19 (6), 1479–1486. https://doi.org/10.1016/j.scient.2012.10.023.
Paz, C., et al., 2013. CFD simulation of a CT scan oral-nasal extra thoracic model. Comput. Methods Multiphase Flow VII, WIT Trans. Eng. Sci. 79, 387–397. https://doi.org/10.2495/MPF130321.
Qi, S., et al., 2014. Computational fluid dynamics simulation of airflow in the trachea and main bronchi for the subjects with left pulmonary artery sling. Biomed. Eng. Online 13 (85). https://doi.org/10.1186/1475-925X-13-85.
Schroder, A., et al., 2015. Advances of PIV and 4D-PTV shake-the-Box for turbulent flow analysis –the flow over periodic hills. Flow Turbul. Combust. 95 (2–3), 193–209. https://doi.org/10.1007/s10494-015-9616-2.
Shur, M.L., et al., 2008. A hybrid RANS-LES approach with delayed-DES and wall-modelled LES capabilities. Int. J. Heat Fluid Flow 29, 1638–1649. https://doi.org/10.1016/j.ijheatfluidflow.2008.07.001.
Smirnov, A., Shi, S., Celik, I., 2001. Random flow generation technique for large eddy simulations and particle-dynamics modeling. J. Fluids Eng. 123 (2), 359–371. https://doi.org/10.1115/1.1369598.
Strohl, K.P., et al., 2012. Mechanical properties of the upper airway. Compr. Physiol. 2 (3), 1853–1872. https://doi.org/10.1002/cphy.c110053.
Sul, B., et al., 2014. A computational study of the respiratory airflow characteristics in normal and obstructed human airways. Comput. Biol. Med. 52, 130–143. https://doi.org/10.1016/j.compbiomed.2014.06.008.
Tian, L., Ahmadi, G., 2012. Transport and deposition of micro-and nano-particles in human tracheobronchial tree by an asymmetric multi-level bifurcation model. J. Comput. Multiph. Flows 4 (2). https://doi.org/10.1260/1757-482X.4.2.159.
Wang, J.X., Wu, J.L., Xiao, H., 2017. Physics-informed machine learning approach for reconstructing Reynolds stress modeling discrepancies based on DNS data. Phys. Rev. Fluids 2 (3). https://doi.org/10.1103/PhysRevFluids.2.034603.
Weibel, E.R., 1963. Morphometry of the Human Lung. Springer Verlag, Berlin. https://doi.org/10.1007/978-3-642-87553-3.
Xi, J., Longest, P.W., 2007. Transport and deposition of micro-aerosols in realistic and simplified models of the oral airway. Ann. Biomed. Eng. 35, 560–581. https://doi.org/10.1007/s10439-006-9245-y.
Xi, J., Longest, P., Martonen, T., 2008. Effects of the laryngeal jet on nano- and microparticle transport and deposition in an approximate model of the upper tracheobronchial airways. J. Appl. Physiol. 104 (6), 1761–1777. https://doi.org/10.1152/japplphysiol.01233.2007.
Xi, J., Kim, J., Si, X.A., Zhou, Y., 2013. Diagnosing obstructive respiratory diseases using exhaled aerosol fingerprints: a feasibility study. J. Aerosol Sci. 64, 24–36. https://doi.org/10.1016/j.jaerosci.2013.06.003.
Yang, D., Shen, L., 2009. Characteristics of coherent vertical structures in turbulent flows over progressive surface waves. Phys. Fluids 21. https://doi.org/10.1063/1.3275851.
Yang, X.L., et al., 2006. The effect of inlet velocity profile on the bifurcation COPD airway flow. Comput. Biol. Med. 36 (2), 181–194.
Zenklusen, A., Kuhn, S., Rudolf von, Rohr P., 2012. Structural dissimilarity of large-scale structures in turbulent flows over wavy walls. Phys. Fluids 24. https://doi.org/10.1063/1.4719778.
Zhang, Y., Finlay, W.H., 2005. Measurement of the effect of cartilaginous rings on particle deposition in a proximal lung bifurcation model. Aerosol Sci. Technol. 39, 394–399. https://doi.org/10.1080/027868290945785.
Zhang, T., Gao, B., Zhou, Z., Chang, Y., 2016. The movement and deposition of PM2.5 in the upper respiratory tract for the patients with heart failure: an elementary CFD study. Biomed. Eng. Online 15. https://doi.org/10.1186/s12938-016-0281-z.
Zheng, Z., et al., 2017. Computational fluid dynamics simulation of the upper airway response to large incisor retraction in adult class I bimaxillary protrusion patients. Sci. Rep. 7, 45706. https://doi.org/10.1038/srep45706.